CONEM 2022
CONGRESSO NACIONAL DE ENGENHARIA MECÂNICA
TERESINA - PI

ABCM
XI CONGRESSO NACIONAL DE ENGENHARIA MECÂNICA
DE 07 A 11 DE AGOSTO DE 2022, TERESINA-PI, BRASIL

FAILURE ANALYSIS OF DOT-39 NON-REFILLABLE REFRIGERANT CYLINDERS

Giovani Silveira de Magalhães Martins, giovani.martins@t2f.ufsc.br[1]
Leonel Edward Beckedorff, leonel.b@t2f.ufsc.br[1]
Kleber Vieira de Paiva, kleber.paiva@t2f.ufsc.br[1]
Jorge Luiz Goes Oliveira, jorge.goes@t2f.ufsc.br[1]

[1] Thermal Fluid Flow Group – T2F, Department of Mobility Engineering, Federal University of Santa Catarina, Joinville, SC, Brazil.

Abstratct: *DOT-39 refrigerant cylinders are low-pressure vessels, used in industrial, commercial and consumer markets as well as in medical applications. These vessels are non-reusable and equipped with a non-refillable one-way hermetic leak-stop valve to prevent refilling. Refilling is considered unsafe and illegal. However, the discarded refrigerant reservoir promotes heavy metal pollution. For the sake of sustainability and pollution prevention, DOT-39 cylinder reutilization demands appraisal. DOT-39 refrigerant cylinders have been evaluated from the fatigue perspective in a test bench. A hydraulic-pneumatic pump was employed to pressurize the cylinder samples with water. The samples were instrumented at the main weld zone (with rosette strain gauges at circumferential and longitudinal directions) and at the torospheric region (with three-axis strain gauges at 0º/45º/90º). Strain gauge measurements were used to determine local equivalent von Misses stresses. The fatigue life of DOT-39 samples was assessed with loads varying from ambient to service pressure (1.5 to 2.5 MPa), emulating their service conditions. Setup parameters were adjusted to promote a slow propagation failure due to crack propagation speed being disturbed by the rate of stress tensor change. The cyclic pressure loads lasted a total of 18 second. The experiments were carried out continuously until failure occurred. Eleven cyclic tests were carried out with the test pressure (Pt) below the upper typical operating pressure. Failure locations due to fatigue were found at welded regions, predominantly at the main weld zone, regardless of lower stress levels. Stress-life diagrams and experimental strength reduction factors at the critical welded locations were obtained based on ASME rules (Sec. VIII, Div. 2). At critical welded locations, fatigue strength reduction factors were determined: between 4 and 5 for the main weld zone at the cylinder center, between 2 and 3 at the valve and tube system and nearly 3 at the pressure relief dimple; DOT-39 cylinders can endure over 700 typical working cycles.*
Keywords: *Fatigue life, DOT-39 refrigerant cylinders, welded regions, fatigue strength reduction factors.*

1. INTRODUCTION

DOT-39 refrigerant cylinders are low-pressure vessels, used in industrial, commercial and consumer markets as well as in medical applications. These cylinders are often used for refrigerant applications and contain refrigerant gases such as R12, R22, R134A, R404A, R500 and R502. These vessels are non-reusable and equipped with a non-refillable one-way hermetic leak-stop valve to prevent refilling (49 CRF, 2012). Refilling is considered unsafe and illegal. However, the discarded refrigerant reservoir promotes heavy metal pollution. For the sake of sustainability and pollution prevention, DOT-39 cylinder reutilization demands appraisal.

DOT rules normalize service and test pressures. The service pressure is the working pressure once the cylinder is filled, whereas the test pressure is a given applied pressure, after which the permanent volume expansion of the refrigerant cylinder cannot exceed 10 percent of the original measured volume (Kisioglu *et al*., 2001). Typical operating pressure ranges nearly from 1.5 to 2.5 MPa for cylinders with a nominal internal diameter and wall thickness equal to 241.3 and 0.81 mm, respectively (Kisioglu *et al*., 2005). The burst pressure is the maximum pressure a cylinder can hold without bursting and it was investigated by Kisioglu (2005). The latter investigated the preferential failure locations induced by the burst pressure by finite element analysis (FEA) and by experiments. However, no investigation attempts have been performed regarding fatigue and preferential failure locations induced by cyclical loads to the best of our knowledge.

In this study, the fatigue life of DOT-39 non-refillable refrigerant cylinders was investigated. Cyclical pressure loads varying from 1.5 up to 2.5 MPa are applied to cylinder samples. Equivalent von Mises stresses are determined by employing strain gauges and pressure transducer devices. An analytical model based on ASME VIII-2 (2015) was developed to create stress-life diagrams. Failure locations induced by fatigue are determined.

2. MATERIALS AND METHODS

2.1. DOT-39 Refrigerant Cylinders

DOT-39 refrigerant cylinders are torispherical-bottomed shell cylinders; see Fig. 1. They consist of cylindrical shells with four dimples located at the bottom symmetrically and circumferentially about the axis of symmetry. A pair of handles are welded at the cylinder top, surrounding a tubing-valve system. A pressure relief dimple is located at the torispherical head over the top knuckle (49 CRF, 2012). Project recommendations are provided by ASME, Section VIII, Div. 1.

DOT-39 cylinders are manufactured within three categories according to their internal diameters, ID: 190.5, 241.3 and 304.8 mm. Each category presents wall thickness, t, ranging from 0.02 to 0.1 in. This investigation only concerns cylinders with a nominal internal diameter and wall thickness equal to 241.3 and 0.81 mm, in that order. Typical design characterizations such as knuckle and crown radius, and the length of the cylindrical shell (L) have been provided by references [Kisioglu *et al.*, 2001; Kisioglu *et al.*, 2005; Kisioglu, 2005). Finally, these cylinders are examined as thin-walled vessels, since t/ID < 0.025, and as shallow cylinders, once L/2 < ID.

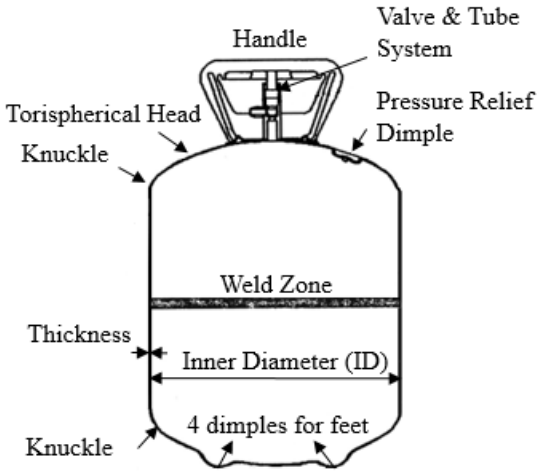

Figure 1. Illustration of the DOT-39 refrigerant cylinder. Schematic adapted from Kisioglu *et al.* (2005).

The manufacturing process consists of welding two shells together at the middle circumferentially about their axis of symmetry. Besides the main weld zone, welding structures are found around the tubing-valve system and nearby the pressure relief dimple. The welding areas are potential failure locations in fatigue processes, as will be demonstrated here.

2.2. Cylinder properties

DOT-39 cylinders are manufactured from SAE-1008 steel, appropriate for metal forming process. During the stamping process, typical material properties, e.g. tensile yield strength (TYS) and ultimate tensile strength (UTS), can be modified, particularly at the weld zone. Heat transfer during the welding process affects microstructure and therefore material properties. TYS and UTS typical values for SAE-1008 are 200 and 334 MPa, in that order (Kisioglu, 2000). Due to the hardening process, Kisioglu (2005) obtained increasing TYS and UTS values at the weld zone: 488 and 585 MPa, respectively.

In this work stress levels imposed on the samples were smaller than YTS and UTS. Only the Young Modulus is crucial for fatigue analysis. Despite the modifications of the true stress-strain curves on the plastic regime, the former researchers observed similar Young Modulus for the elastic regime. Consequently, a typical Young Modulus for SAE-1008 steel, 202 GPa, is adopted.

2.3. Experimental Setup

Figure 2 shows the test facility. The test arrangement can be divided into a pressurization bench (Fig. 2, right) and a test section: a security banker which houses testing samples (Fig. 2, left). The pressurization bench was designed by Flutrol Company and it aims at controlling cyclic pressure loads. The maximum allowed pressure is 20 MPa. The bench consists of a hydro-pneumatic pump, model ASF-35, fed by an air line at 7 bar, a pressure relief system and valves which allow pressure control.

The samples were instrumented at the main weld zone (with rosette strain gauges at circumferential and longitudinal directions) and at the torospheric region (with three-axis strain gauges at 0º/45º/90º). After connecting the pressurization hose to a sample, the latter is placed inside a security bunker for safety reasons. Deformation and pressure measurements are attained by the data acquisition system (Lynx ADS1800). Hydrostatic pressure loads are measured with a pressure transducer (PX401 Series Omega). The transducer measuring range is 0-5 MPa, and the uncertainty is 0.5 % of full scale.

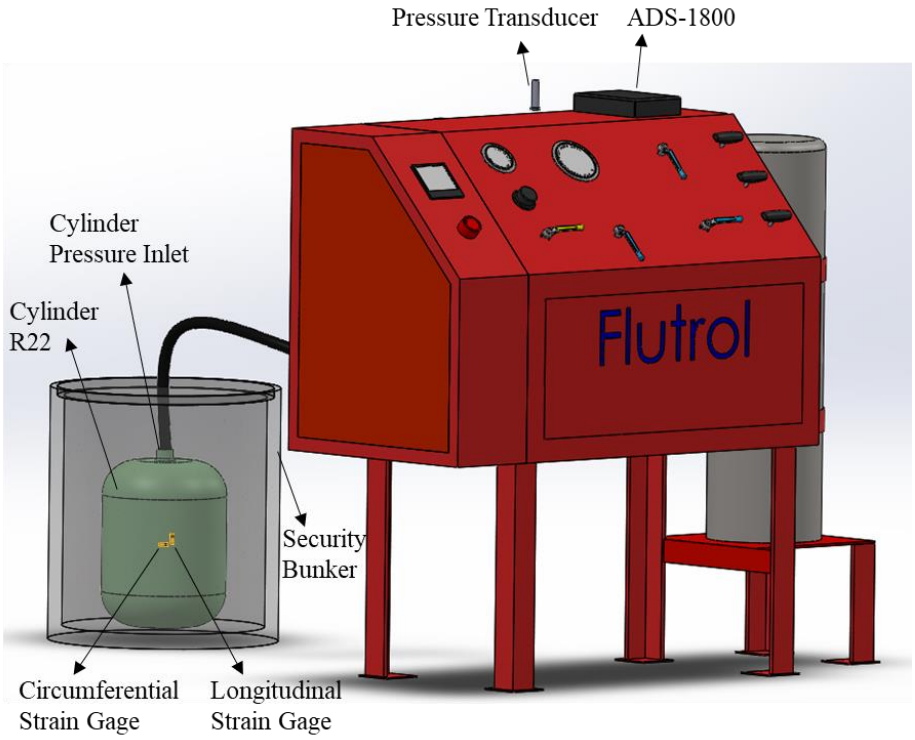

Figure 2. Schematics of the experimental setup: test section (left) and pneumatic/hydraulic setup (right).

2.4. Test Procedure

Eleven cyclic tests were carried out with the test pressure (Pt) below the upper typical operation pressure (Pt = 1.5; 2 and 2.5 MPa). Five experiments occurred with Pt = 2 MPa and five, with Pt = 2.5 MPa. Only one experiment occurred with Pt = 1.5 MPa to confirm the increasing useful life with reduced stress levels as well as to preserve the experimental setup.

Before exposing the samples to cyclic loads, the weld joints were inspected following the recommendations of the ASME Code, Section VIII, Div. 2, Annex 6-A. Visual, penetrating liquid and leak detector inspections were performed as non-destructive tests.

Setup parameters were adjusted to promote a slow propagation failure due to crack propagation speed being disturbed by the rate of stress tensor change. The cyclic pressure loads lasted a total of 18 seconds: 10s to pressurize from ambient pressure to test pressure; 0.5s for depressurization; and 7.5s at constant ambient pressure. The experiments were carried out continuously until failure occurred.

3. STRESS DETERMINATION

3.1. Pressure Approach

The DOT-39 geometry effect on stress estimation at the main weld zone can be accounted for by thin-walled vessel approximation:

$$\sigma_L = \frac{pr}{2t} \tag{1}$$

$$\sigma_\theta = \frac{pr}{t} \tag{2}$$

where σ is stress, p, the static pressure, r, the vessel radius and t, the vessel thickness. The subscripts L and θ stand for longitudinal and circumferential directions. It is assumed that: a) material properties are isotropic; b) pressure loads promote minor deformation and c) the wall thickness is negligible compared to the vessel radius. According to Timoshenko and Woinoswsky-Krieger (1959), assumptions a) and b) suffice for applying an isotropic linear elastic model, whereas assumption c) implies negligible stress variation along with the wall thickness.

Stress estimations at the torispherical head for longitudinal and circumferential directions, $\sigma_{L,max}$ and $\sigma_{\theta,max}$, respectively, are accounted for by Bickell & Ruiz (1967) equations:

$$\sigma_{L,max} = 1.293\frac{pr}{2t} \tag{3}$$

$$\sigma_{\theta,max} = 1.032\frac{pr}{t} \tag{4}$$

The increase in longitudinal and circumferential stresses occurs due to the combination of membrane and flexural stresses.

3.2. Strain Approach

At the weld zone, rosette strain gauges were positioned in accordance with longitudinal and circumferential directions. With the deformation measurements and by applying Hooke's law, it is possible to attain stresses at the weld zone as:

$$\sigma_L = E.\frac{\varepsilon_L + v.\varepsilon_\theta}{(1-v^2)} \tag{5}$$

$$\sigma_\theta = E.\frac{\varepsilon_\theta + v.\varepsilon_L}{(1-v^2)} \tag{6}$$

where E and v are the Young's Modulus and Poisson's ratio, respectively.

Due to the geometric complexity of the torospheric head, the main directions are unknown, requiring the use of triaxial strain gauges (0º, 45º, 90º). The principal normal stresses (σ_p, σ_q) are computed at the measurement point as:

$$\sigma_{p,q} = \frac{E}{1-\nu}.\frac{\varepsilon_0 + \varepsilon_{90}}{2} \pm \frac{E}{\sqrt{2}\,(1+\nu)}.\sqrt{(\varepsilon_0 - \varepsilon_{45})^2 + (\varepsilon_{90} - \varepsilon_{45})^2} \tag{7}$$

where the subscripts 0º, 45º and 90º stand for deformations at the concerning directions.

4. ASME SEC. VIII, DIV. 2

The allowable fatigue cycles for the DOT-39 cylinder were determined using experiments, following the ASME practices (2015) for failure evaluation due to cyclic loading. Strain measurements at chosen failure locations (welded regions) were used to determine local stresses. The fatigue strength reduction factors can be evaluated with effective total equivalent stress amplitude ($S_{alt,k}$) and the number of cycles data to failure. A similar approach as applied in Martins *et al*. (2020) has been followed.

The equivalent stress tensor ($\Delta\sigma_{ij,k}$) is determined according to the equipment operation, at peak (a) and valley (b) values of fatigue duty cycles. The effective equivalent stress ranges ($\Delta S_{P,k}$) are obtained using von Mises stress criteria:

$$\Delta\sigma_{ij,k} = {}^{a}\sigma_{ij,k} - {}^{b}\sigma_{ij,k} \tag{8}$$

$$\Delta S_{P,k} = \frac{1}{\sqrt{2}}\left[\left(\Delta\sigma_{11,k} - \Delta\sigma_{22,k}\right)^2 + \left(\Delta\sigma_{11,k} - \Delta\sigma_{33,k}\right)^2 + \left(\Delta\sigma_{22,k} - \Delta\sigma_{33,k}\right)^2 + 6\left(\Delta\sigma^2{}_{12,k} + \Delta\sigma^2{}_{13,k} + \Delta\sigma^2{}_{23,k}\right)^2\right]^{0.5} \tag{9}$$

where subscripts 1, 2, and 3 are coordinates.

Using the range of primary plus secondary plus peak equivalent stress, the effective alternating equivalent stress can be computed from Equation (10) considering both a fatigue strength reduction factor (K_f) and a fatigue penalty factor ($K_{e,k}$):

$$S_{alt,k} = \frac{K_f K_{e,k} \Delta S_{P,k}}{2} \tag{10}$$

The fatigue strength reduction factor is related to the weld quality and the surface conditions of the equipment. It represents the ratio between the fatigue strength of a component without a discontinuity or weld joint and the fatigue strength of that same component with a discontinuity or weld joint (smooth bar). The experimental determination of the fatigue resistance reduction factors must be in accordance with ASME Sec VIII - Div. 2 (2015), section 5-F.3.10.

The fatigue penalty factor accounts for the type of material and maximum temperature allowable in the cycles. It is used to compensate for progressive deformation due to alternating stresses, when notching effects are not sufficient to

characterize the effects of plastic deformation associated with discontinuities; see Langer (1972), Tagart (1972), Adams (2006), Slagis (2005, 2006), Asada *et al*. (2001), Merend and Parsons (1995) and Chattopadhyway (2005).

The factor $K_{e,k}$ is obtained as:

$$K_{e,k} = 1 \qquad \text{for } S_n \le S_{PS} \tag{11}$$

$$K_{e,k} = 1 + \frac{1-n}{n(m-1)}\left(\frac{\Delta S_{n,k}}{S_{PS}} - 1\right) \qquad \text{for } S_{PS} < S_n \le mS_{PS} \tag{12}$$

$$K_{e,k} = \frac{1}{n} \qquad \text{for } S_n \le mS_{PS} \tag{13}$$

The constants m and n depend on the material properties and the hardening process. The value of *m* and *n* employed in this study were 2.0 and 0.2, respectively. The primary plus secondary equivalent stress range, S_n, is equal to the equivalent stress range. The allowable limit, $S_{PS,}$ depends on material properties, calculated as the maximum value between three times the allowable stress, S, and two times the yield strength, S_y; $S_{PS} = \max [3S, 2S_y]$.

The alternating equivalent stress amplitude is used to compute the allowable number of cycles, N. The procedure is described in the Annex 3-F of the referred ASME code. The smooth bar design fatigue curves are polynomial functions that depend on the material properties (C_1 to C_{11}) and the stress amplitude. Equations (14-16) are provided to determine the number of permissible cycles:

$$N = 10^{X} \tag{14}$$

$$X = \frac{C_1 + C_3 Y + C_5 Y^2 + C_7 Y^3 + C_9 Y^4 + C_{11} Y^5}{1 + C_2 Y + C_4 Y^2 + C_6 Y^3 + C_8 Y^4 + C_{10} Y^5} \tag{15}$$

$$Y = \left(\frac{S_{alt,k}}{C_{us}}\right).\left(\frac{E_{FC}}{E_T}\right) \tag{16}$$

where E_{FC}, $E_{T,}$ C_{us} are: the elasticity modulus used to establish the design fatigue curve, the elasticity modulus at average temperature and conversion factor, respectively. Add to this, $C_{us} = 1$ for unit of stress in MPa.

5. RESULTS

5.1. Stresses

Table 1 presents stress estimations at the main weld zone and at the torispherical head for three service pressures: 1.5, 2.0 and 2.5 MPa.

Table 1. DOT-39 geometry effect on stress estimations by thin walled vessel approximation at the main weld zone, and by Bickell & Ruiz (1967) equations at the torispherical head.

Peak pressure [MPa]	Stresses at the main weld zone: thin walled vessel approximation [MPa]				Stresses at the torispherical head: Bickell & Ruiz equation [MPa]				$\frac{(\Delta SP, k)_{head}}{(\Delta SP, k)_{weld,zone}}$
	σ_L	σ_θ	σ_θ / σ_L	$(\Delta S_{P,k})_{weld,zone}$	σ_{Lmax}	$\sigma_{\theta max}$	$\sigma_{\theta max} / \sigma_{Lmax}$	$(\Delta S_{P,k})_{head}$	
1.5	82.3	164.5	2	142.5	106.4	169.8	1.6	148.6	1.043
2.0	109.7	219.4	2	190.0	141.8	226.4	1.6	198.1	1.043
2.5	137.1	274.2	2	237.5	177.3	283.0	1.6	247.7	1.043

According to Bickell & Ruiz (1967), stress levels increase because of the complex torispherical geometry that works as a type of stress concentration factor; see Tab. 1. Moreover, stress levels become less heterogeneous: note that the stress ratio σ_θ / σ_L is reduced to 1.6 at the torispherical head. The theoretical ratio of von Mises stresses at the torispherical head and at the main weld zone, $(\Delta S_{P,k})_{head} / (\Delta S_{P,k})_{weld,zone}$, is 1.043. Through error propagation analysis, von Mises stress uncertainties were inferior to 4.45% of the calculated value.

Table 2 presents deformation measurements at the main weld zone and at the torispherical head for three service pressures: 1.5, 2.0 and 2.5 MPa. Table 3 presents stresses as obtained by strain gauge measurements. Average stress uncertainty was nearly 5 MPa of the calculated value.

Table 2. DOT-39 geometry effect on deformation at the main weld zone (rosette strain gauge) and at the torispherical head (three-axis strain gauge).

Peak pressure [MPa]	Deformation at the main weld zone: [μm/m]		Deformation at the torispherical head [μm/m]		
	ε_L	ε_θ	ε (0º)	ε (45º)	ε (90º)
1.5	207.14	656.53	361.28	10.94	468.46
2.0	280.42	904.50	444.58	6.19	606.39
2.5	347.38	1124.67	604.19	-5.92	764.53

Table 3. DOT-39 geometry effect on stresses computed with deformation measurements.

Peak pressure [MPa]	Stresses at the main weld zone: experiments [MPa]				Stress at the torispherical head: experiments [MPa]	$\frac{(\Delta SP,k)_{head}}{(\Delta SP,k)_{weld,zone}}$
	σ_L	σ_θ	σ_θ / σ_L	$(\Delta S_{P,k})_{weld,zone}$	$(\Delta S_{P,k})_{head}$	
1.5	89.7	159.5	1.78	138.5	189.3	1.37
2.0	111.5	199.7	1.79	173.3	244.3	1.40
2.5	138.3	272.7	1.97	236.2	322.6	1.36

At the weld zone, stresses estimated with the thin-walled vessel approximation were in close agreement to the results obtained with stresses computed with deformation measurements. The σ_θ / σ_L ratio has been reduced from 2 to values in the range 1.78 and 1.97. The reduction in σ_θ/σ_L results from inadequacies to the thin-walled pressure vessel theory. For example, the vessel material is not perfectly isotropic. Variations in the cylinder wall thickness may occur as well as stress concentration effects due to the weld bead. These shortages contribute to reduce the difference between longitudinal and circumferential stresses in the experiments.

As expected, stresses obtained by means of strain gauge measurements were higher at the torispherical head. von Mises stress ratio, $(\Delta S_{P,k})_{head} / (\Delta S_{P,k})_{weld,zone}$, ranged from 1.36 to 1.40; see Tab. 3. These results suggest that Bickell & Ruiz equations do not suffice to predict stresses at torispherical head: $(\Delta S_{P,k})_{head} / (\Delta S_{P,k})_{weld,zone}$ is 1.043; see Tab. 1. The following arguments possibly explain this difference: mechanical properties vary significantly in the torispherical region due to the stamping process and intense wall thickness variations occur as well as noteworthy stress concentration factors.

Finally, it is possible to infer that the DOT-39 Ultimate Tensile Strength (UTS) and Tensile Yield strength (TYS) are clearly superior to the ones for pure SAE-1008 material; see stress values at the torispherical head in the service pressure equal to 2.5 MPa. Stresses computed with the aid of strain gauges will be applied in the fatigue life section.

5.2. Failure Locations

All experiments failed in welded regions; see Fig. 3: a) five at the main weld zone; b) three at the weld around the tubing-valve system and c) three nearby the weld surrounding the pressure relief dimple.

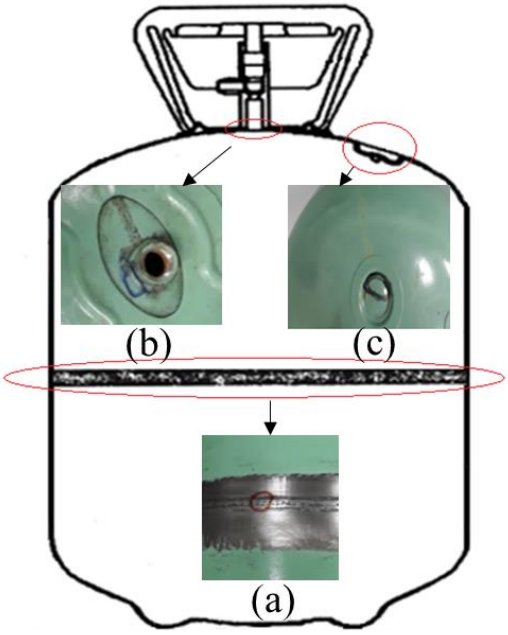

Figure 3. Failure locations of DOT-39 vessels exposed to cyclic loads.

Table 4 presents the fatigue life of DOT-39 samples: failure location and number of cyclic loads. The increase in service pressure leads to a reduction in the number of cycles to failure, as expected. With the peak pressure set to 1.5 MPa, failure occurred at the tubing-valve system once the number of cycles was equal to 9936. With the peak pressure set to 2.0 and 2.5 MPa, failures occurred in three locations. With the peak pressure set to 2.0 MPa, failures at the main weld zone occurred with a reduced number of cycles as compared to failures at the tubing-valve system and at the pressure relief dimple.

Table 4. Fatigue life of DOT-39 samples: failure location and number of cyclic loads.

Peak pressure [MPa]	Main weld zone	Tubing-valve system	Pressure relief dimple
1.5		9936	
2.0	1651 / 2478 / 2670	3882	5558
2.5	752 / 2203	734	1617 / 2258

Data in Tab. 4 suggest heterogeneous welding structures at the DOT-39 samples. The low quality of the manufacturing process may be related to cost reductions, once the devices are discarded after unfilled. Remarkably, failures occurred at the main weld zone regardless of the inferior stress levels observed at this region. The extended length-scale of the welding process surrounding each shell may impose a low-quality weld at this region: interruptions during the welding process may contribute to the presence of contaminants and oxides, resulting in elevated stress concentration factors. Furthermore, metal inert gas (MIG) and metal active gas (MAG) welding processes may promote porosity because of the absorption of nitrogen, oxygen and hydrogen in the molten weld pool (AWS, 2004). Regardless of manufacturing concerns, it is still noteworthy that these devices could endure over 700 cycles with typical service pressures.

5.3. Fatigue Life

Fatigue strength reduction factors for the DOT-39 samples are determined using a model based on ASME standard (Section 4). The values of these factors depend directly on the weld quality and surface finish, ranging from 1 to 4: low numbers indicate high weld quality. It was assumed that the stress levels at the torispherical head were representative for the tubing-valve system and the pressure relief dimple.

Figures 4 and 5 present the effect of DOT-39 weld quality on fatigue life. The results are plotted considering the Von Mises equivalent stresses by the number of cycles to failure. Experimental results were compared to analytical data where the fatigue strength reduction factor (K_f) are: 1, 2, 3 and 4. Figure 4 presents results at the main weld zone and Fig. 5, at the torispherical head (tubing-valve system and pressure relief dimple).

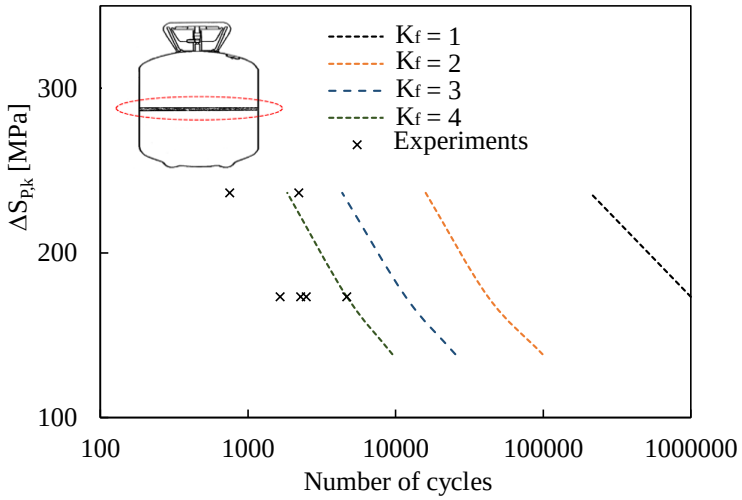

Figure 4. Effect of weld quality at the main weld zone on the DOT-39 fatigue life.

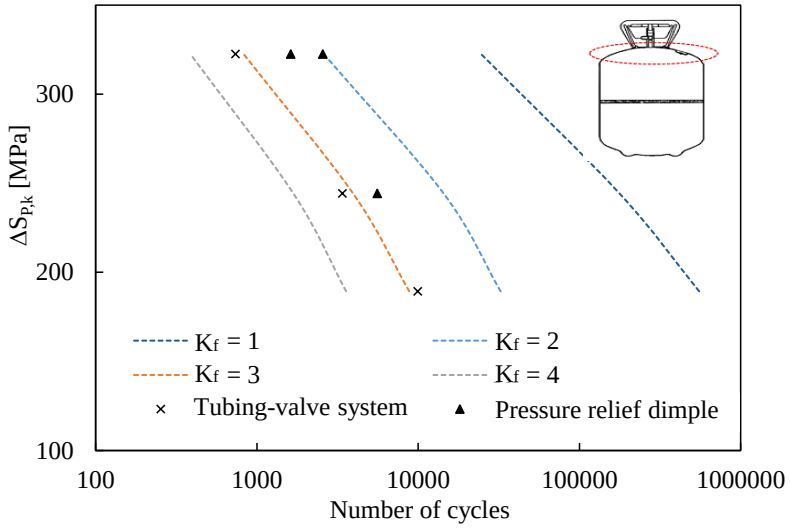

Figure 5. Effect of weld quality at the torispherical head (tubing-valve system and the pressure relief dimple) on the DOT-39 fatigue life.

One can also obverse in Fig. 4 that the fatigue life declines with increasing fatigue strength reduction factor. It can be seen that the fatigue life is nearly 10^5 with $K_f = 1$, 10^4 with $K_f = 2$ and 10^3 with $K_f = 4$ at the main weld zone for $\Delta S_{P,k} \sim$ 250 MPa. Experimental values approach the theoretical ones with K_f ranging between 4 and 5 at the main weld zone (see Fig. 4), and with K_f ranging between 2 and 3 at the pressure relief dimple (see Fig. 5). At the tubing-valve system, experimental results are in close agreement with the theoretical ones for $K_f = 3$. It is important to emphasize that the actual number of cycles to failure ranges from 10^3 to 10^4, characterizing low-cycle fatigue.

The different trends in $\Delta S_{P,k}$ x Number of cycles curves observed in Fig. 4 and 5 are explained as follows. The fatigue penalty factor (K_e) affects the computation of the number of cycles to failure. The factor K_e is determined in accordance with the vessel material and the maximum equivalent stress (S_n). With reduced stresses, $K_e = 1$ and increases to 1.3 once von Mises stresses approach the material tensile strength. At the main weld zone, $K_e = 1$ for all $\Delta S_{P,k}$ values. At the torispherical head, K_e increased from 1 to 1.3 for the upper $\Delta S_{P,k}$ range, modifying the $\Delta S_{P,k}$ x Number of cycles curvature and reducing the fatigue life.

6. CONCLUSIONS

The fatigue life of samples of DOT-39 non-refillable refrigerant cylinders was evaluated with loads varying from 1.5 to 2.5 MPa, emulating their service conditions. Pressure transducer and strain gauge measurements were used to determine local stresses. Stress-life diagrams were obtained based on ASME rules (Sec. VIII, Div. 2). The main conclusions are highlighted as follows:

- Longitudinal and circumferential stresses determined at the DOT-39 weld zone were in close agreement with theoretical stresses for thin-walled vessels. Stress concentration factors reduced the ratio of circumferential to longitudinal stresses from 2 to nearly 1.8;
- At the torispherical head, von Mises equivalent stress is nearly 38% higher than at the weld zone;
- Failure locations due to fatigue were found at welded regions, predominantly at the main weld zone, regardless of lower stress levels. Failures can also occur at other welded regions: at the valve and tube system, and at the pressure relief dimple;
- At critical welded locations, fatigue strength reduction factors were determined: between 4 and 5 for the main weld zone at the cylinder center, between 2 and 3 at the valve and tube system and nearly 3 at the pressure relief dimple;
- With the peak inner pressure set to 1.5, 2.0 and 2.5 MPa, DOT-39 cylinders can endure over 9,936, 1,651 and 734 cycles, respectively.

7. REFERENCES

49 CFR (Code of Federal Regulation), 2012. Part 178 Subpart C, Office of Federal Registrar, National Archives and Records Administration, US Government Printing Office, Washington, DC.

Adams. S.A., 2006. "*An alternate simplified elastic-plastic analysis method: Technical Support Doccument*". ASME Code Correspondence. Revision 1.

American Society of Mechanical Engineers, 2015. "*ASME Boiler and Pressure Vessel Code, Section VIII: Rules for Construction of Pressure Vessels.*" Division 2.

American Welding Society (AWS), 2004. "*AWS D1.1/D1.1M: Structural Welding Code - Steel.*" 2 ed. Miami: American Welding Society, 541 p.

Asada. S., Nakarmura. T., Asada. Y., 2001. "*Evaluation of conservatism in the simplified elastic-plastic analysis using analytical results – Part 2: Proposal of a new Ke-Function". Pressure Vessels and Piping: Design and Analysis*. Vol 407. Pressure Vessels and Piping Codes and Standards. ASME, pp. 255-262.

Bickell, M. B., and Ruiz, C., 1967. "*Pressure Vessels Design and Analysis*", Macmillan, London, UK, 198 p.

Chattopadhyway. S., 2005. "*Pressure Vessels. Design and Practice*". CRC Press Boca Raton. FL. pp. 129-139.

Kisioglu, Y., 2000. "*A New Design Approach and FEA Modeling for Imperfect End Closures of DOT Specification Cylinders*", Ph.D. Dissertation, The Ohio State University, 319 p.

Kisioglu, Y., 2005. "*Effects of weld zone properties on burst pressures and failure locations*" *Turkish J. Eng. Environ. Sci.*, Vol. 29, no. 1, pp. 21–28.

Kisioglu, Y., Brevick, J. R. and Kinzel, G. L., 2001. "*Determination of Burst Pressure and Location of the DOT-39 Refrigerant Cylinders*," *J. Press. Vessel Technol*.,Vol. 123, no. 2, 240 p.

Kisioglu, Y., Brevick, J. R. and Kinzel, G. L., 2005. "*Bottom End-Closure Design Optimization of DOT-39 Non-Refillable Refrigerant Cylinders*", *J. Press. Vessel Technol.*, Vol. 127, no. 2, 112 p.

Langer. B. F., 1972. "*Design of Pressure Bessels for Low-Cycle Fatigue". Pressure Vessels and Piping: Design and Analysis*. ASME. New York, pp. 107-120.

Martins, G. S. M., Silva, R. P. P., Beckedorff, L. E., Monteiro, A.S., Paiva, K. V., Oliveira, J. L. G., 2020. "*Fatigue Performance Evaluation of Plate and Shell Heat Exchangers*", *I. J. of Pressure Vessels and Piping*, vol 188, pp. 104237.

Merend. A., Parsons. L.S., 1995. "*A comparison of the simplified elastic-plastic strain concentration factor Ke. of the ASME Boiler and Pressure Vessel Code with Experimental and Analytical Results*". PVP-Vol 313-1. International Pressure Vessels and Piping Codes and Standards: Volume 1 – Current Applications. ASME, pp 415-421.

Slagis. G.C., 2005. "*Meaning of Ke in Design-by-Analysis Fatigue Evaluation*". *Pressure Vessels and Piping: Design and Analysis*. ASME, Vol. 3, pp. 433-450.

Slagis. G.C., 2006. "*ASME Section III Design-by-Analysis Criteria Concepts and Stress Limits*". Journal of Pressure Vessel Technology. Vol. 128. ASME, pp. 25-32.

Tagart. W.S., 1972. "*Plastic fatigue analysis of pressure components*". Pressure Vessels and Piping: Design and Analysis. ASME. New York, pp. 209-226.

Timoshenko, S. Woinoswsky-Krieger, S., 1959. *"Theory of Plates and Shells"*. 2 ed, McGraw-Hill, Inc., New York, 558 p.

8. COPYRIGHT RESPONSIBILITY